

Doctoral Dissertation

Evaluation of intercellular lipid lamellae in the stratum corneum by polarized microscopy

Asada Naoki

Program of Data Science
Graduate School of Science and Technology
Nara Institute of Science and Technology

Supervisor: Prof. Shigehiko Kanaya
Computational Systems Biology Laboratory

Submitted on September 2, 2022

A Doctor's Dissertation
submitted to Graduate School of Science and Technology,
Nara Institute of Science and Technology
in partial fulfillment of the requirements for the degree of
Doctor of SCIENCE

Naoki Asada

Thesis Committee:

Professor Shigehiko Kanaya

(Supervisor, Division of Information Science)

Associate Professor Naoaki Ono

(Co-supervisor, Division of Information Science)

Evaluation of intercellular lipid lamellae in the stratum corneum by polarized microscopy

Asada Naoki

Abstract

Background: Intercellular lipids contain a lamellar structure that glows in polarized images. It could be expected that the intercellular lipid content based on the luminance values derived from polarized images of the stratum corneum. Therefore, we developed a method for a simple and rapid evaluation of the intercellular lipid content. Herein, we demonstrated a relationship between the luminance value and the amount of ceramides, one of the main components of intercellular lipids.

Materials and Methods: Samples from the stratum corneum were collected from the forearm using slides with a pure rubber-based adhesive, which did not produce unnecessary luminescence under polarizing conditions. Images were analyzed using luminance indices. Positive secondary ion peak images and polarized and brightfield images were obtained by time of flight–secondary ion mass spectrometry (ToF-SIMS) and a polarized microscope, respectively. The concentrations of ceramide and protein amount were measured by high-performance liquid chromatography and bicinchoninic acid protein assay after microscope imaging. Images and quantitative values were used to construct evaluation models based on a convolutional neural network (CNN).

Results: The highlighted area of the polarized image was correlated with the overlap with the area where ceramide-derived peak was detected ($r^2 = 0.27$; $p < 0.001$). Based on the polarized and brightfield images, the actual ratio correlated with the index of the amount of ceramides per unit of the stratum corneum ($r^2 = 0.33$; $p = 0.0013$) and with the ratio predicted from the evaluation of the CNN-based model of the polarized images ($r^2 = 0.42$; $p < 0.001$).

Conclusion: Imaging the same area of the sample using a polarizing microscope and by ToF-SIMS showed the contribution of the presence of ceramide to polarization brightness. The method that we developed allows a simple and rapid evaluation of the intercellular lipid content based on luminance calculated from polarized images of the stratum corneum, suggesting the possibility with a large number of specimens.

Keywords: Convolutional neural network, Polarized microscope image, Computer modeling, Skin barrier, Skin physiology/structure

Doctoral Dissertation, Graduate of Science and Technology, Nara Institute of Science and Technology, September 2, 2022

Contents

Chapter 1: Introduction	1
1.1 The role and basic structure of the skin	1
1.2 Intercellular lipids in the stratum corneum that play a role in barrier function	1
1.3 Functional and structural evaluation of the stratum corneum	3
1.4 Evaluation method for the structure of intercellular lipids	4
1.5 Evaluation method for the composition of intercellular lipids	5
1.6 Evaluation method for the skin using machine learning	6
1.7 Purpose of this study	6
Chapter 2: Materials and Methods	12
2.1 Selection of the adhesive and base materials and development of sampling tools	12
2.2 Time of flight–secondary ion mass spectrometry analysis	12
2.3 Ceramide analysis using ImageJ and deep learning	13
Chapter 3: Results	21
3.1 ToF-SIMS analysis using ImageJ	21
3.2 Ceramide estimation based on luminance indices	21
3.3 Ceramide amount regression using deep learning	22
Chapter 4: Discussion	27
Chapter 5: Conclusion	30
Research Achievement	32
Acknowledgment	33
Reference	34

List of figures

Figure 1 Skin structure	7
Figure 2 Ceramide metabolism	8
Figure 3 Structure and nomenclature of ceramides	9
Figure 4 Transmission electron micrograph of lamellar structure of intercellular lipid in stratum corneum	10
Figure 5 Long-period lamellar structure and short-period lamellar structure of intercellular lipids in stratum corneum	11
Figure 6 Brightfield and polarized microscope images	17
Figure 7 A schematic illustration of skin ceramide analysis	18
Figure 8 Number of samples	19
Figure 9 The network architecture	20
Figure 10 ToF-SIMS imaging analysis	23
Figure 11 Comparison of the observed and predicted protein and ceramide contents and their ratios	24
Figure 12 Comparison of the observed and predicted protein and ceramide contents and their ratios	25
Figure 13 Feature areas highlighted by Grad-CAM	26
Supplementary Figure S1 ToF-SIMS, polarized and brightfield images	31

Chapter 1: Introduction

1.1 The role and basic structure of the skin

To perform tasks, an organism requires a tissue that separates it from the external environment. For mammals, including humans, the skin plays a protective role against external stimuli and has adequate flexibility that does not interfere with the behavior of the organism (i.e., the mammal). The mammalian skin consists of the epidermis, dermis, and subcutaneous tissue. The average thickness of the epidermis is approximately 0.1 mm, depending on its location in the body. Keratinocytes are cells that comprise more than 95% of the epidermis, and they are pushed upward by cell division in the basal lamina, which is in contact with the dermis. During the process of differentiation, metabolism, composition, and structure of the cells change; the stratum spinosum, stratum granulosum, and stratum corneum are formed in order from the basal layer. The stratum corneum is the most superficial layer that eventually exfoliates and falls off as plaque. Its cellular nucleus disappears, a mechanism called denucleation. This series of cell morphological changes is called epidermal turnover.

1.2 Intercellular lipids in the stratum corneum that play a role in barrier function

Skin moisture is controlled by the epidermis, which inhibits water evaporation from the body surface and retains water in the stratum corneum. The stratum corneum is approximately 20 μm thick and composed of 15 layers of brick-like cells held together by intercellular lipids like a mortar. The stratum corneum contains natural moisturizing factors, mainly amino acids, and retains moisture. On the other hand, intercellular lipids, which play the role of mortar, serve as one of the important epidermal moisturizing factors and function as barriers to water evaporation and foreign matter invasion by filling the gaps between corneocytes (Fig. 1). In plants, the barrier lipids are made up of wax esters and alkanes (hydrocarbons), whereas in terrestrial mammals, ceramides (50%), cholesterol ester (15%), cholesterol (5%), and fatty acids (20%) comprise the intercellular lipids in the stratum corneum.^{1,2}

Keratinocytes below the inner nuclear layer produce intercellular lipids and ceramides, majority of which are metabolized to glucosylceramides and sphingomyelin that either form the cell membrane (Fig. 2)³ or transported to the lamellar bodies in the keratinocytes.⁴ Lamellar bodies also contain cholesterol and other substances that are necessary for the stratum corneum and responsible for their storage and delivery to the stratum corneum. When the lamellar body enters the stratum corneum, it fuses with the cell membrane on the stratum corneum side and releases its contents into the intercellular space of the stratum corneum.⁵ The released lipids are hydrolyzed by enzymes into ceramides, fatty acids, and cholesterol, which form the lamellar structure that influence the epidermal barrier function.

Ceramides in the stratum corneum are composed of 12 classes, which are a combination of three types of fatty acids and four types of sphingosine (sphingoid base) (Fig. 3).^{6,7} Recently, ultrasensitive analysis methods for ceramide species are used to analyze the distribution of carbon numbers in the carbon chains of fatty acids and sphingosines⁸ and metabolic enzymes.⁹ The carbon numbers of free fatty acids are also widely distributed and include both saturated and unsaturated fatty acids. Regardless of their molecular diversity, regular structures appear in intercellular lipid aggregates. Staining the stratum corneum with osmium oxide or ruthenium oxide will help visualize the ultrathin sections under a transmission electron microscope, exhibiting stripe patterns in the spaces between the corneocytes.^{10, 11, 12} The pattern forms a periodic structure of approximately 13 nm in some areas and approximately 6 nm in others^{13, 14, 15} (Fig. 4). X-ray and neutron diffraction also demonstrated the same results, which will be shown later.

1.3 Functional and structural evaluation of the stratum corneum

The stratum corneum, formed by epidermal turnover, plays a particularly important role in skin barrier function.^{1, 2}

The division rate of keratinocytes depends on aging, body part, and skin diseases such as dry skin and psoriasis. It also corresponds to the stratum corneum turnover, therefore making possible the assessment of the skin condition by examining the stratum corneum turnover. One method is observation of the morphology of the stratum corneum cells by tape stripping. In the case of hyperkeratosis, nucleated cells stand out and their area is smaller than that of non-nucleated cells.¹⁶ The turnover time is 7 days in the dry skin area

of atopic dermatitis patients and 14 days in normal skin, with the cell area approximately 15% smaller than normal.¹⁷ In the turnover of a normal skin, the balance between exfoliation and regeneration is maintained at a constant level. Conversely, in the stratum corneum, the turnover is imbalanced and function is impaired, and hence the barrier function is also impaired.

To evaluate barrier function of the skin, the transepidermal water loss (TEWL) is measured. TEWL is an index expressed as the amount of water ($\text{g}/\text{m}^2/\text{h}$) per unit time and unit area that evaporates from the inside to the outside of the body. As, by definition, the barrier function inhibits water evaporation, TEWL is focused on moisture transpiration suppression. However, TEWL increases with blood flow, temperature, and perspiration of the skin, thus requiring subjects to rest in an environment with constant temperature and humidity. Changes in TEWL are influenced by aging and skin diseases. Particularly, TEWL decreases slightly with age,¹⁸ which is actually due to a delay in turnover and a thicker volume of poorly functioning stratum corneum, making the barrier function appear higher among the older individuals. One of the effects of aging includes the reduction of circulatory functions such as skin blood flow and skin tone, resulting in lower water content just below the stratum corneum and lower TEWL. In atopic dermatitis patients, TEWL is high even in eczema-free areas, and TEWL has been related to the ceramide content in the stratum corneum.¹⁹ Since the diagnosis of atopy is time-consuming, measurement of ceramide content may be a diagnostic aid. However, measurement of ceramide content is labor intensive and difficult to provide to a large number of patients.

To evaluate the arrangement of stratum corneum cells in the skin, the tape stripping method is employed. The stratum corneum is stripped with a tape to evaluate the degree of insufficiency of keratinization based on the stratified state of the collected stratum corneum; however, this does not directly correspond to barrier function.²⁰ An *in vivo* confocal laser scanning microscope (CLSM) is used in fluorescence mode to allow a detailed three-dimensional observation of the adhesive state between stratum corneum cells.^{21, 22} In this method, the stratum corneum cells of the skin coated with 0.1% fluorescein solution are used. The barrier function is considered good if the shape of individual stratum corneum cells is clearly observed and deteriorated if the outline of stratum corneum cells is blurred and the edges are flattened. However, as both tape stripping method and CLSM are imaging methods, their results are not quantitative even

though they enable observation of the state of the stratum corneum construction at the cellular level.

1.4 Evaluation method for of the structure of intercellular lipids

On transmission electron microscopy, intercellular lipids in the stratum corneum have a lamellar structure¹⁴ (Fig. 4). X-ray scattering is a more microscopic method that can analyze the periodic structure and packing method of intercellular lipids, which play the role of mortar. Small-angle X-ray scattering can evaluate the periodic structure of X-ray intercellular lipids. Long and short lamellar structures have repeat distances of approximately 13 and 6 nm in the human stratum corneum, respectively.^{23, 24} The long periodicity phase (LPP) is abundant in a mouse stratum corneum, while the short periodicity phase (SPP) is abundant in human stratum corneum.^{24, 25} Ceramide 1 (ceramide molecule with fatty acid attached to the ω -position of ω -hydroxy ceramide) is essential for the formation of LPP.^{26, 27} Water is present between the lamellae of SPPs (Fig. 5).^{28, 29} This is in agreement with the experimental results of neutron diffraction, which is another method to evaluate the periodic structure.³⁰ Meanwhile, wide-angle X-ray scattering is performed to evaluate the lateral lipid packing structure of intercellular lipids. The hydrocarbon chains of intercellular lipids are regularly packed in their interior. In the mouse stratum corneum, the Hex structure (the hexagonal lattice, gel phase) is the major component of LPP, and conversely, the Ort structure (the orthorhombic packing (crystalline phase)) is the major component of SPP.³¹ Both X-ray scattering and neutron diffraction require relatively large samples (excised skin) and require experiments at large-scale synchrotron radiation facilities.

Electron diffraction is another method to analyze the packing structure of intercellular lipids that requires a transmission electron microscope of approximately 100 kV. It allows local analysis in a short time and with a small amount of sample (a single exfoliated stratum corneum). By this method, the presence of Hex to Ort in the stratum corneum is increased in patients with atopic dermatitis compared to that in healthy individuals,³² and the changes are associated with reduced skin barrier function as measured by TEWL.³³ However, electron diffraction poses some challenges, such as electron beam damage and charge-up and the need to hold only one stratum corneum cell in a hollow and vacuumed passage for the electron beam to penetrate.

These evaluation methods of the cyclic structure of intercellular lipids in the stratum corneum helps in the evaluation of skin conditions, but these are still limited to experimental use due to these issues.

1.5 Evaluation method for the composition of intercellular lipids

Devices have been developed to evaluate skin condition based on intercellular lipid content. Confocal Raman spectroscopy has been used in a laboratory setting as a noninvasive *in vivo* optical method.^{34, 35} However, despite its accuracy and good reproducibility, this method is now generally expensive and has difficulty in measuring a wide range as the device measures only one point that focuses on the object. Alternatively, commercially available measuring devices for ceramide, which is one of the main components of intercellular lipids, consider water content in the stratum corneum and skin indices based on touch. However, despite being sufficiently easy to use and availability for skin evaluation and patient counseling, these devices do not measure the actual ceramide content.

The ceramide content in the stratum corneum decreases with age,^{36,37} and this decrease has been correlated inversely with TEWL.¹⁹ Therefore, ceramides maintain a favorable skin condition. Current methods for measurement of the actual ceramide content include the use of a calibration curve of the reference standard from thin layer chromatography (TLC) and a more accurate quantification method based on high-performance liquid chromatography (HPLC). The lipid composition is altered in atopic dermatitis patients compared to that in healthy individuals.³⁸ However, both TLC and HPLC methods extract lipids from a stratum corneum strip using a tape³⁹ and consume the entire sample, thereby making subsequent observations and analyses of the stratum corneum strip after staining challenging. In addition, as these methods require delicate sample preparation and expensive analyzers, we need less time-consuming and simpler methods.

1.6 Evaluation method for the skin using machine learning

Machine learning is an artificial intelligence technique that utilizes machines and programs to mimic intelligent human behaviors. In recent years, machine learning has been reportedly used a number of dermatological studies, including in the diagnosis of

skin lesions such as skin cancer.^{40, 41}

A convolutional neural network (CNN) is a machine learning method that simulates the processing of biological neurons and is frequently used in image recognition.^{42, 43}

For consumer use applications, a system uses random forest to evaluate the effectiveness of pore coverage,⁴⁴ or CNN to capture signs of aging through selfies and suggest anti-aging strategies.⁴⁵ Overhead photographs of the face are used to evaluate the performance of makeup products and bare skin with no makeup. However, studies on machine learning evaluation of stripped stratum corneum are few, none of them have investigated the barrier structure itself using polarized microscope images, which allow direct evaluation of the lamellar structure.

1.7 Purpose of this study

In this study, our aim was to develop a method for simple and objective measurement of the intercellular lipid content that is nondestructive to the samples and does not require an expensive analyzer. Moreover, we aim that this novel method will be used not only for research but also as a service and provide additional morphological observation and chemical analysis while preserving morphology without destroying the stratum corneum sample. This method was designed to be offered on the sales floor and as a diagnostic aid for atopy. In this study, we considered for sample collection the tape stripping method, which is feasible and noninvasive for individuals. For a quick and simple evaluation, the stratum corneum was directly observed without any pretreatment both before and after collection, and the polarized brightness of intercellular lipid lamellar structures were analyzed.^{46, 47} Ceramide was used as an indicator of the intercellular lipid lamellar structure, for its relation to the skin barrier function.

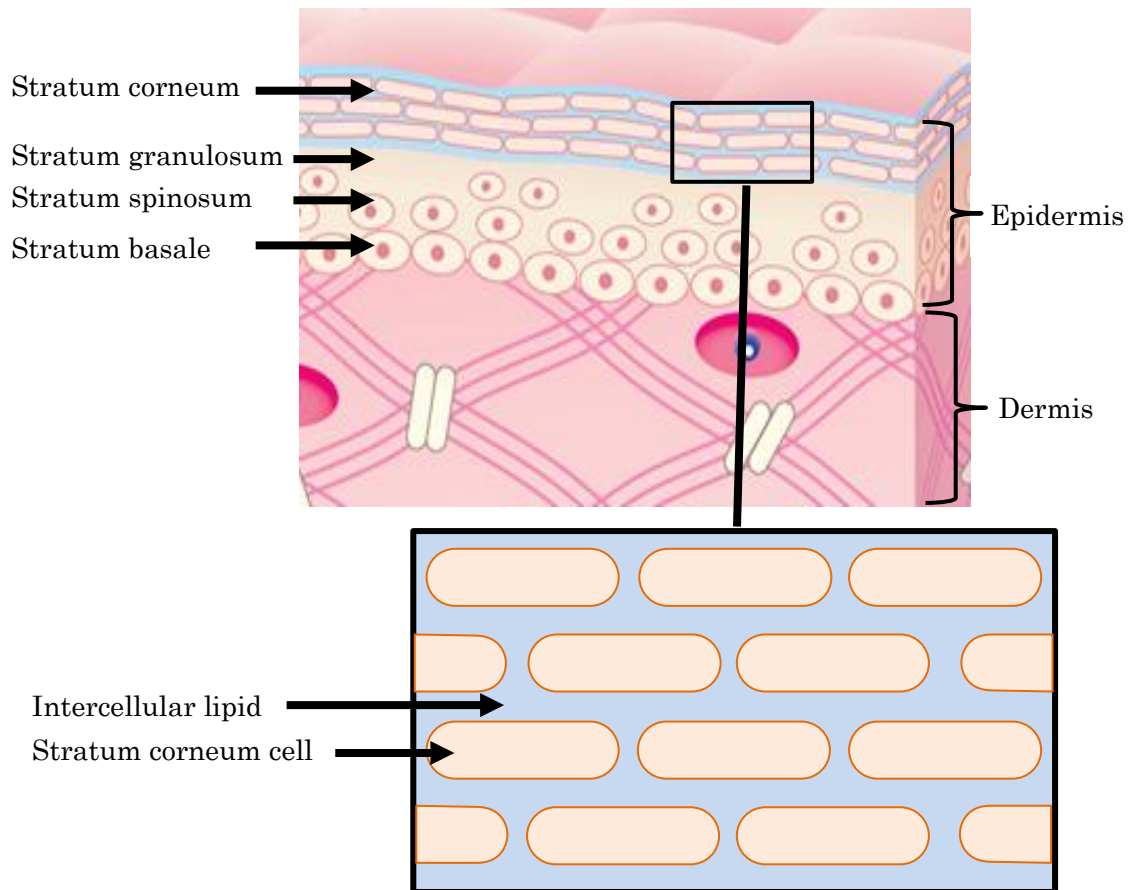


Figure 1. Skin structure. The epidermis consists of the stratum corneum, stratum granulosum, stratum spinosum, and stratum basale in order from the outside. In the stratum corneum, intercellular lipids fill the spaces between stratum corneum cells.

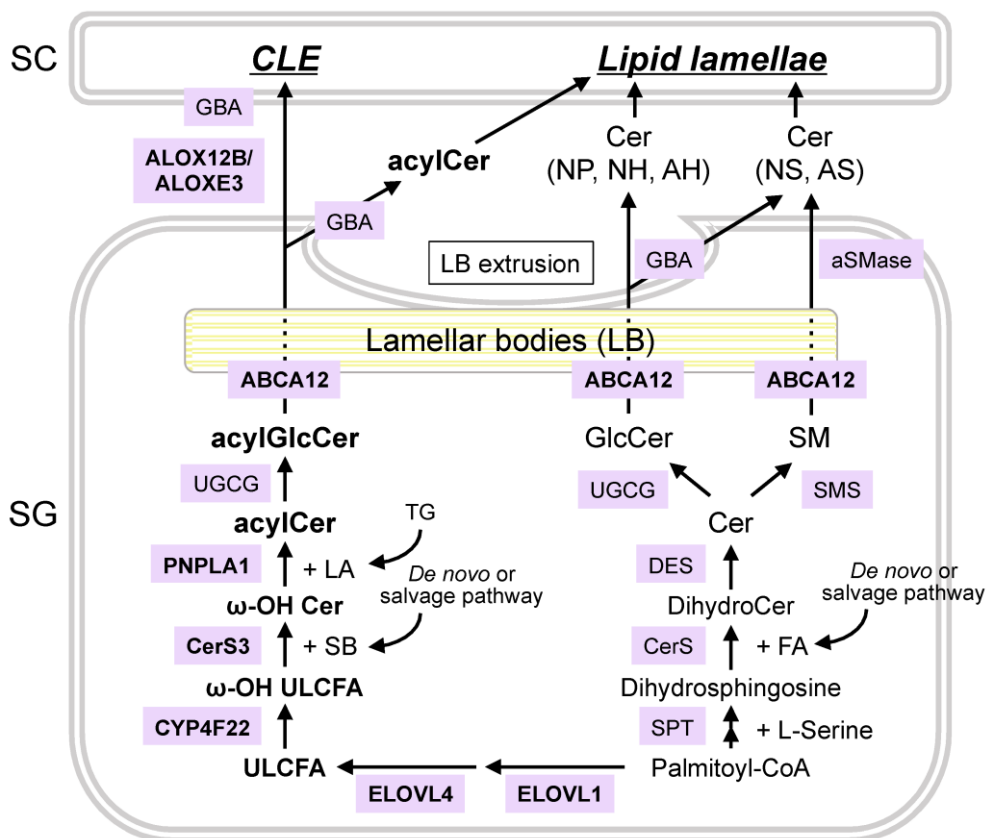


Figure 2. Ceramide metabolism.³ Synthetic pathways of epidermal ceramides (Cer). The de novo pathway begins with the condensation of L-serine and palmitoyl coenzyme A (-CoA) to form 3-ketosphinganine. Glucosylceramide (GluCer) and sphingomyelin (SM) are converted to ceramide by glucocerebrosidase and sphingomyelinase, respectively. A portion of ceramide is hydrolyzed to fatty acids (FAs) and sphingosine bases by ceramidase and used again as a substrate for ceramide synthesis. (Salvage pathway)

GlcCer, glucosylceramide; SM, sphingomyelin; ULCFA, ultra-long-chain fatty acid; acylCer, acylceramide; SB, sphingoid base; LA, linoleic acid; TG, triglyceride; SPT, serine palmitoyl-CoA transferase; CerS, ceramide synthase; DES, desaturase; UGCG, UDP-glucose ceramide glucosyltransferase; SMS, sphingomyelin synthase; ABCA12, ATP-binding cassette transporter 12; GBA, β-glucocerebrosidase; aSMase, acid sphingomyelinase; ELOVL, elongase of very long-chain fatty acid; CYP, cytochrome P450; PNPLA1, patatin-like phospholipase domain-containing 1; ALOX12B, 12R-lipoxygenase; ALOXE3, epidermis-type lipoxygenase-3.

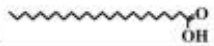

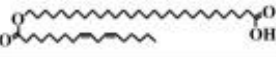
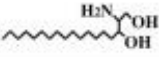
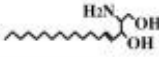
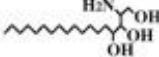
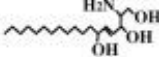
Fatty acid	Non-hydroxy fatty acid [N]	α -hydroxy fatty acid [A]	Esterified ω -hydroxy fatty acid [EO]
Sphingoid			
Dihydrosphingosine [DS] 	CER[NDS]	CER[ADS]	CER[EODS]
Sphingosine [S] 	CER[NS]	CER[AS]	CER[EOS]
Phytosphingosine [P] 	CER[NP]	CER[AP]	CER[EOP]
6-hydroxy sphingosine [H] 	CER[NH]	CER[AH]	CER[EOH]

Figure 3. Structure and nomenclature of ceramides.⁶ Ceramides (CER) in the stratum corneum are composed of 12 classes, which are a combination of three types of fatty acids and four types of sphingosine (sphingoid base). In the normal human stratum corneum, 11 classes have been confirmed to be present except for CER[EODS].

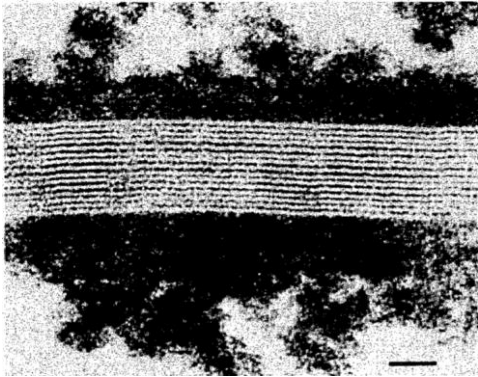


Figure 4. Transmission electron micrograph of lamellar structure of intercellular lipid in stratum corneum.¹⁴ Distinct bands originate from the stratified structure of intercellular lipids. Bar: 25 nm.

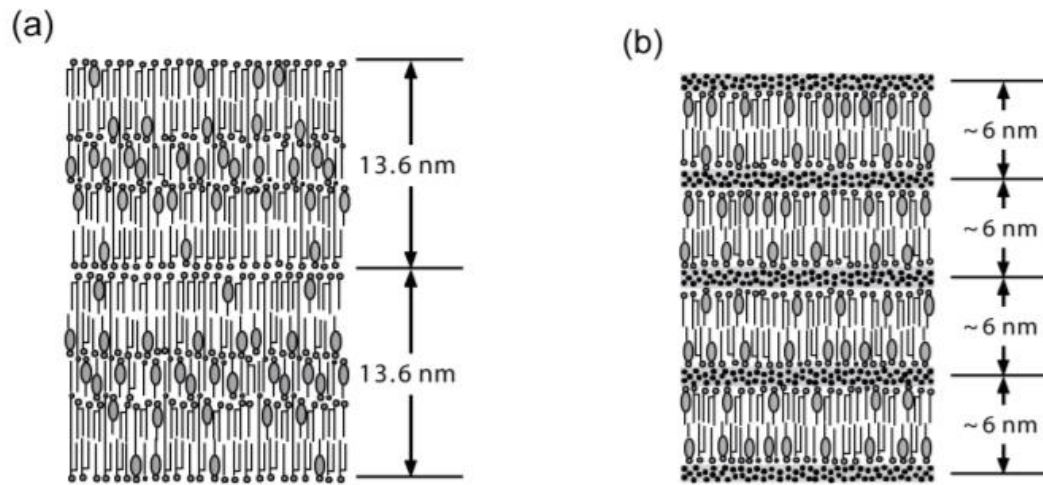


Figure 5. (a) Long periodicity phase (LPP) and (b) short periodicity phase (SPP) of intercellular lipids in the stratum corneum.²⁹ In the human stratum corneum, long and short lamellar structures have repeat distances of approximately 13 and 6 nm, respectively. Water is present between the lamellae of SPPs. Ceramides: with the circle, two lines indicating a branch chain. Free fatty acid: with a circle, one line indicating the chain. Cholesterol: perfectly round and oval. Water layer: black dots.

Chapter 2: Materials and Methods

2.1 Selection of the adhesive and base materials and development of sampling tools

Measurement of luminance of a lamellar structure in the stratum corneum^{48, 49} using sampling tapes was difficult because the tape materials, such as resins and cellulose, in the adhesive layer and the base layer cause unnecessary luminescence under polarizing conditions. Therefore, we began developing optimal sampling tools to extract luminance data for the lamellar structure because rubber-based adhesives do not have an ordered crystal structure.

A stratum corneum strip was collected by tape and was observed under polarized light as it was or attached to a glass slide without being transferred (Fig. 6). We evaluated various types of adhesives while paying attention to the background under polarizing conditions. Slides with pure rubber-based adhesive suppress the observation of unnecessary luminescence and turned blackest. Based on this observation, we developed a tool for sampling the stratum corneum as follows: A mixture of a pure rubber-based adhesive which are commercially available (Rubber Cement Non-Toluene; Maruni Industry, Japan) and hexanes (1:9) was applied evenly onto a uncoated glass slide as the base material (Star Frost Slide Glass, water glass, edged, white, 5116; Muto Pure Chemicals Co., Ltd., Japan), which had an approximate thickness of 12.5 $\mu\text{L}/\text{cm}^2$ (200 μL per slide glass) using a micropipette; thereafter, the slide was dried in a fume hood at room temperature for 6 hours. With this tool, the stratum corneum can be directly observed without the need to transfer. Further, the low stickiness inhibits multiple peeling, and the amount of stratum corneum does not change significantly depending on the sampling pressure.

2.2 Time of flight–secondary ion mass spectrometry analysis

Next, to verify the presence of ceramide in the highlighted area of the polarized image, samples from the stratum corneum strip were obtained from the forearm of a healthy volunteer. For the time of flight–secondary ion mass spectrometry (ToF-SIMS), a focused

beam of high energy ions was irradiated on the sample surface, resulting in the emission of secondary ions, which were analyzed in a ToF analyzer (ToF-SIMS5, ION-ToF GmbH, Germany) to provide molecular information about the sample surface. For SIMS analysis, 30 kV Bi³⁺⁺ was used as the primary ion and a beam current of 0.2 pA. Sixteen scans of 500 × 500 μm samples were tested. Positive secondary ions were used to identify the endogenous ceramides present in the stratum corneum.⁵⁰

Transmitted light brightfield and polarized TIFF images (1600 × 1200 pixels) of the same samples were obtained using a polarized microscope equipped with crossed polarizers (BX53, Olympus, Japan). A halogen lamp built into the microscope and ACHN10XP were used as the light source and the objective lens, respectively. The images were analyzed using ImageJ (Wayne Rasband, National Institutes of Health, USA) and converted to 8-bit and merged using “Merge Channels.” Green represented the positive secondary ion peak image; blue, the polarized image; and red, the brightfield image. A plot profile was used to analyze the merged images. The data of the pixel intensities along a line within the images were displayed in a two-dimensional graph.

2.3 Ceramide analysis using ImageJ and deep learning

The main concept examined is illustrated schematically in Fig. 7. The method comprised five components.

1. Stratum corneum sampling

A total of 28 stratum corneum specimens from 15 subjects (5 men and 10 women; age range, 28–59 years) were obtained from the volar side of both forearms. Sample collection of the stratum corneum was performed five times per forearm at the same site. The skin was firmly pressed for 5 seconds using five of the sampling slides mentioned above by the same individual (five layers of samples, Figs. 8A–8B).

2. Imaging of stripped stratum corneum (observation)

From each layer of the sample, brightfield and polarized images of the stratum corneum were obtained using a polarized microscope. Twenty-five images were randomly captured at 100× magnification while avoiding overlap of the fields. Therefore, the 125 brightfield and polarized images per arm were taken for each method (Figs. 8C–8D).

3. HPLC and bicinchoninic acid protein assay

Preparation of ceramide fractions of the samples

The stratum corneum sampling tool was immersed in hexanes (8 mL/ glass slide) and sonicated until the applied materials, including the adhesive, completely came off. The glass slide was taken out, the sample was centrifuged at 3000 rpm for 10 minutes, and the supernatant was removed. After adding 10 mL of hexanes to the precipitates, the sample was suspended and centrifuged at 3000 rpm for 10 minutes. The supernatant was removed, and the precipitants with 2 mL of hexanes were collected. The collected liquid was centrifuged at 3000 rpm for 10 minutes, the supernatant was removed, and the hexanes were completely removed by exposure to nitrogen gas with heating. The end product was the ceramide fraction.

The ceramide fraction was mixed with 20 μ L of 10- μ M C16 sphingosine in chloroform/methanol (2:1, v/v) and 400 μ L of chloroform/ methanol (2:1, v/v) as the internal standard solution; this mixture was allowed to stand at 37°C for 2 hours. After sonication, the sample was centrifuged at 15000 rpm for 10 minutes, the supernatant was collected, and the solvent was removed by exposure to nitrogen gas. SCDase (0.5 mU in 2 μ L) was added to the sample dissolved in 27 μ L of 25-mM sodium acetate buffer (pH 5.5) containing 5-mM CaCl₂ and 2.0% TritonX-100. The mixture was left to stand at 37°C for 2 hours, and the reaction was stopped with 200 μ L of chloroform/ methanol (2:1, v/v). Water (15 μ L) was added to the chloroform/ methanol solution, which was mixed well and centrifuged. The lower layer was taken out, and the solvent was removed by exposure to nitrogen gas then dissolved in 120 μ L of ethanol. The ethanol solution was mixed with the OPA reagent, which contained 0.1 mL of ethanol, 10 mg of OPA, 20 μ L of 2-mercaptoethanol, and 9.9 mL of 3% (w/v) boric acid buffer (pH 10.5); this mixture was incubated at 70°C for 120 minutes. The OPA reagent (15 μ L) was added to the ethanol solution and incubated at 70°C for 60 minutes. The sample was centrifuged at 15,000 rpm for 10 minutes, and the supernatant was transferred to a glass vial. A 15- μ L aliquot of the sample was injected into an HPLC column using an autosampler.⁵¹

High-performance liquid chromatography analysis

The analysis was conducted by reverse-phase HPLC. A Shimadzu LC-20 series analyzer connected to a Shimadzu RF-10A fluorescence detector was used. The column was a Capcellpak C18 (Osaka Soda, Osaka, Japan), which had an inner diameter of 4.6 mm \times

150 mm. In this LC/ RFD system, a binary pump was connected to two mobile phases (A: 0.1% acetic acid and B: methanol with a flow rate of 1 mL/min). The mobile phases were consecutively programmed as follows: A 20% (B 80%) between 0 and 20 minutes; A 0% (B 100%) between 20 and 40 minutes; and an isocratic elution of A 20% (B 80%) from 40 to 50 minutes for column equilibrium, for a total run time of 50 minutes. The injection volume was 5 μ L. The column temperature was maintained at 40 °C. Fluorescence was detected at 440 nm with an excitation wavelength of 335 nm. The total peak area after identification of the internal standard peaks divided by the area of the internal standard peaks was designated as M_{cera} (Fig. 8E).

Quantification of protein in the samples

The insoluble fraction obtained during preparation of the ceramide fraction was used as the protein-containing fraction (three fractions per sample). The protein-containing fraction was mixed well with 50 μ L of sodium lauryl sulfate aqueous solution (3 mg/mL) before adding 450 μ L of water. The proteins were quantified using the TaKaRa BCA Protein Assay Kit, following the manufacturer's instructions. The cumulative amount of protein in the three fractions was regarded as the amount of protein in the sample (M_{prot}) (Fig. 8F).

4. Image analysis using luminance indices

The ceramide content was evaluated from the luminance areas using an image analyzing software ImageJ. The polarized image was converted to 8-bit grayscale, the threshold was set with the preset triangle method, and the number of pixels that had luminance higher than the threshold and the total luminance in the pixels were calculated. The brightfield image was converted to 8-bit, the colors were inverted, the threshold was set with the preset triangle method, and the number of pixels that had luminance higher than that of the threshold and the total luminance in the pixels were calculated.

Using the luminance values and the number of pixels obtained from the brightfield image, the Stripping Index of Amount (SIA), which was a parameter of the amount of the stripped stratum corneum, was calculated by the following equation (1)⁵²:

$$\text{SIA} = (\Sigma \text{ luminance value}) \times (\text{number of pixels}) \quad (1)$$

In addition, using the luminance values and the number of pixels obtained from the polarized image, the Ceramide Index of Amount (CIA), which was a parameter of the amount of ceramide, was calculated by the following equation (2):

$$\text{CIA} = (\Sigma \text{ luminance value}) \times (\text{number of pixels}) \quad (2)$$

All images obtained were analyzed, and the average SIA and CIA for each specimen were calculated. Single regression analyses were performed using the SIA to calculate the M_{prot} using the BCA Kit and using the CIA to calculate the M_{cera} using HPLC. The CIA/ SIA and $M_{\text{cera}}/ M_{\text{prot}}$ were used as the variables for each analysis to confirm the respective correlation coefficients and p values.

5. *Image analysis using deep learning*

We developed an evaluation model from the brightfield and polarized images using deep learning. To evaluate the ceramide content based on the obtained images, we constructed a regression model based on CNN.^{53, 54} Sample image data were resized into 200×150 pixels as the input layer and rescaled its intensity between 0 and 1. A seven-layer convolutional neural network that comprised five convolution layers and two dense layers, including dropout layers after each intermediate output, was constructed (Fig. 9). The input variables were the concatenated pixel matrix of brightfield and polarized images, and the objective variables were the protein content or the ratio of the ceramide to the protein content for the brightfield images and the ceramide content for the polarized images. The three models were trained as regression models using mean squared error as loss functions. We trained each model with 300 epochs using Adam optimizer⁵⁵ (initial learning rate = 0.001) and confirmed that the training was saturated since both the learning curves of training and validation data were converged. The objective variables were scaled to the normal distribution, which had an average of 0 and a variance of 1. Using a total of 125 brightfield and 125 polarized images, which were collected by obtaining data from 25 images (pictures) from each of the five sample layers per specimen, regression analysis was performed with 10-fold cross-validation. The average values obtained were regarded as the predictive values of each specimen.

Moreover, we applied the gradient-weighted class activation mapping (Grad-CAM)⁵⁶ in order to highlight the areas where the images contributed to the regression results. The Grad-CAM is a technique that evaluates the weight of a network that contributes to the regression by back-calculating the derivatives of the values of the feature maps for the final output values. This method is frequently used in the analysis of results obtained from deep learning models, which is usually considered a black box.

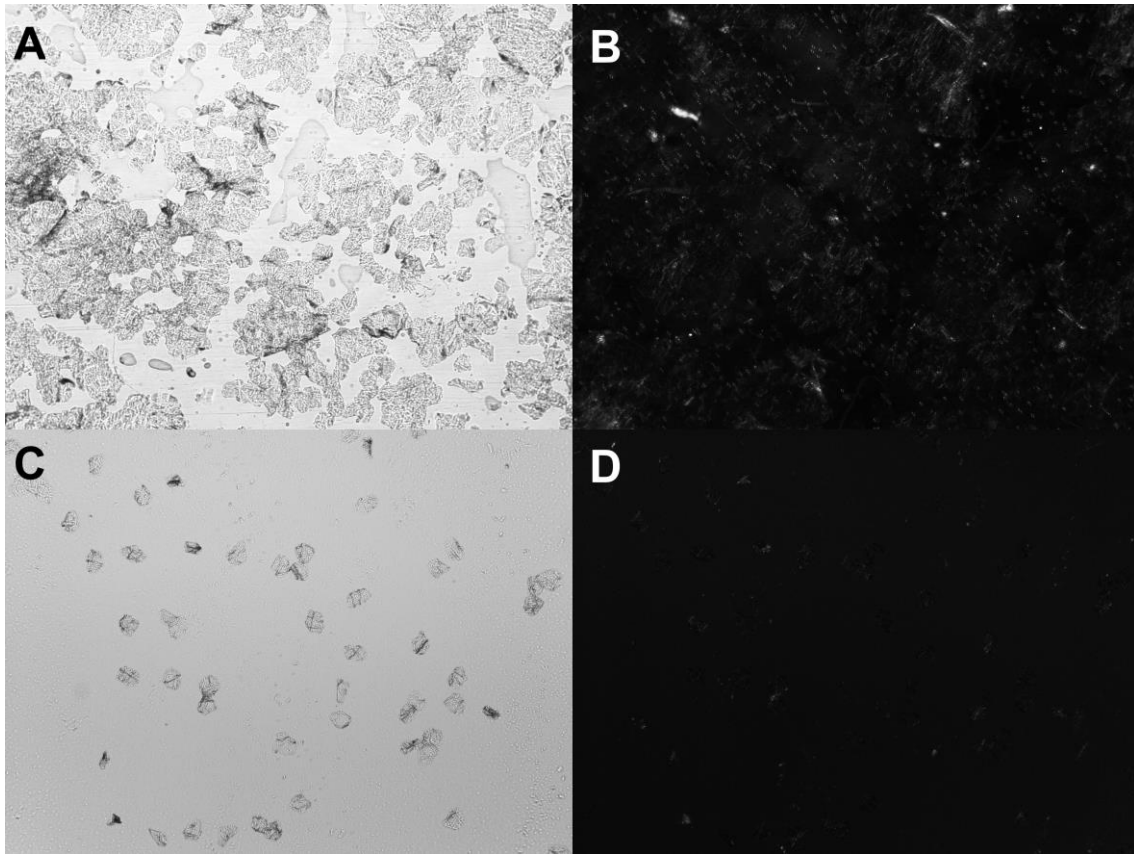


Figure 6. Brightfield and polarized microscope images. A-B: Brightfield and polarized microscope images in the same area obtained using cellophane tape. In image B, a large amount of cellophane-derived unnecessary luminescence was observed. C-D: brightfield and polarized microscope images in the same area obtained using a rubber-based adhesive (100× magnification). In image D, no unnecessary luminescence was observed.

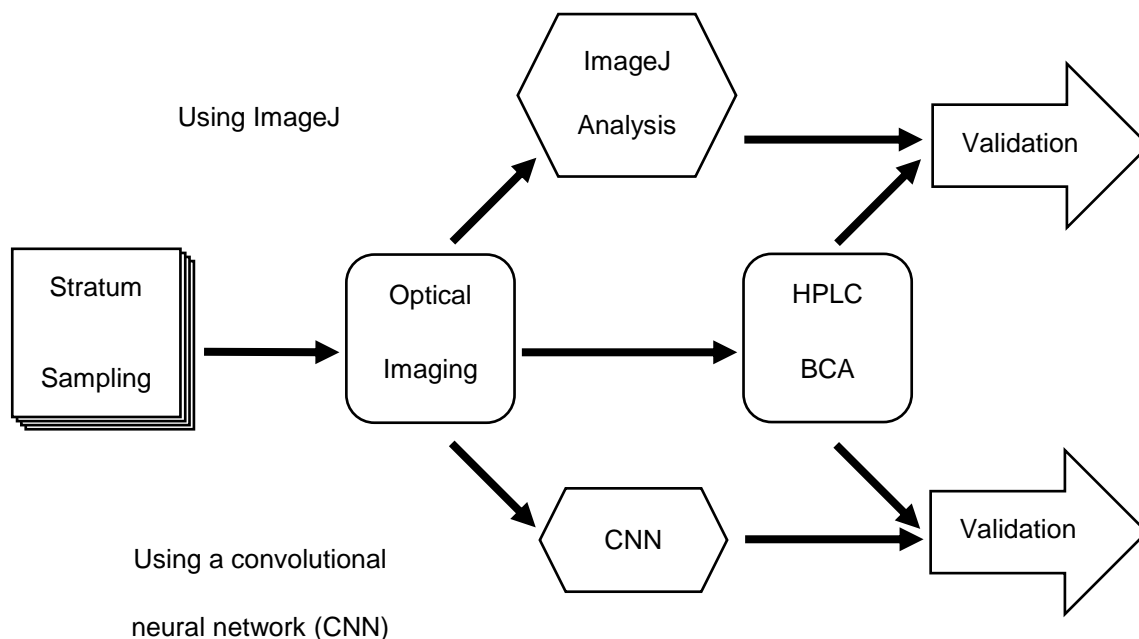


Figure 7. A schematic illustration of skin ceramide analysis. After obtaining samples, optical imaging is performed. Samples after imaging are quantitatively analyzed by HPLC and BCA to obtain ceramide and stratum corneum protein amounts. The samples obtained from the imaging are analyzed by ImageJ and CNN. The results of each image analysis and the results of the quantitative analysis were subjected to regression analysis. Glass slides with stratum corneum samples: with overlapping squares. Imaging and quantitative analyses: with rounded squares. Image analyses: with hexagons. Regression analyses: with thick right arrows. HPLC, high-performance liquid chromatography; BCA, TaKaRa BCA protein assay kit.


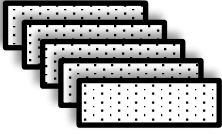

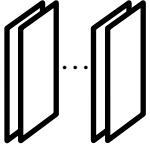
A: Specimens (arms)	B: Layers	C: Polarized images	D: Brightfield images	E: Amount of ceramides	F: Amount of protein
Arm (No. 1) 	5 layers (No. 1–5) 	125 pictures (No. 1–125) (25 pictures×5 layers) 	125 pictures (No. 1–125) (25 pictures×5 layers) 	HPLC (No.1) M_{cera}	BCA (No.1) M_{prot}
...
Arm (No. 28)	5 layers (No. 136–140)	125 pictures (No. 3376–3500)	125 pictures (No. 3376–3500)	HPLC (No.28)	BCA (No.28)

Figure 8. Number of samples. B is stripped from A. C and D are obtained from B using a polarized microscope. E and F are obtained by analysis from B. HPLC, high-performance liquid chromatography; BCA, TaKaRa BCA protein assay kit; M_{cera} , the amount of ceramides in the sample; M_{prot} , the amount of protein in the sample.

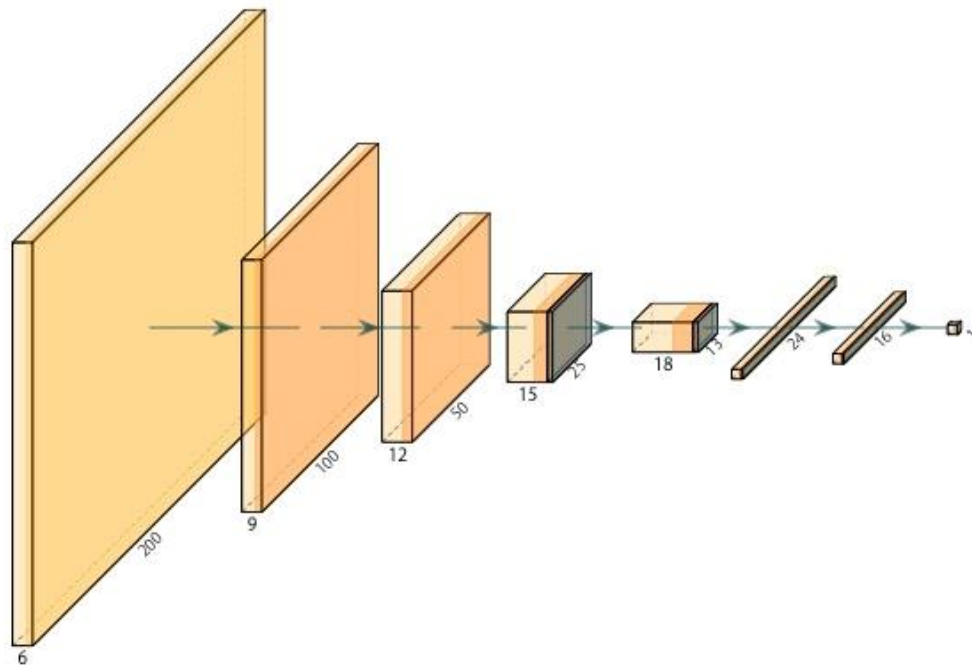


Figure 9. The network architecture. The regression model comprised five convoluted and two fully connected layers. For the convolution filter, the kernel size is 5×5 pixels, the stride is 2 pixels, and the numbers of filters are set to 9, 12, 15, 18, and 24. The feature maps are converted into flat layer and passed into fully connected layers. Each fully connected layer has 16 and 1 output nodes, which is the final regression output. The ReLU activation function is used in each layer, except for the last layer. Dropout layers (drop rate = 0.2) are used on the third and subsequent layer outputs at the time of learning. ReLU, rectified linear unit.

Chapter 3: Results

3.1 ToF-SIMS analysis using ImageJ

In this study, polarization of the stratum corneum exfoliated using the method developed in the present study was confirmed by polarization microscopy in all exfoliated stratum corneum from the first layer to the fifth layer. Upon identification of polarization-causing components, the ceramide-derived peak was detected from the tape stripping sample by ToF-SIMS (Fig. 10A). The obtained polarized images and brightfield images in the same area were merged (Figs. 10B–10D). Analysis by plot profile revealed a correlation between the highlighted area of the polarized image and overlap with the area where ceramide-derived peak ($r^2 = 0.27$; $p < 0.001$) (Fig. 10E). The highlighted area of the ceramide-derived peak (Fig. 10A, green) covered the stratum corneum area (Fig. 10C, red), whereas the highlighted area of the polarized image (Fig. 10B, blue) was within the area of the ceramide-derived peak. Therefore, ceramide was present in the area where the polarization brightness was high. These data were one of several similar results (Supplementary Fig. S1).

In our correlational investigation, data obtained from 28 arms from which samples for the quantification of ceramide and protein content and imaging analysis were used; no issues were noted. Five layers of samples were taken from one arm, and 25 fields of view per layer were recorded to cover most of the collected samples' area, totaling to 125 brightfield and polarized images taken from each arm.

3.2 Ceramide estimation based on luminance indices

An image was taken by observing the stratum corneum exfoliated from the forearm with a polarizing microscope. After imaging, ceramide and protein contents contained in the stratum corneum were quantified using HPLC and evaluated their correlation with the luminance indices computed from the brightfield and polarized images. The single regression analyses found significant positive correlations between the SIA and M_{prot} ($r^2 = 0.21$, $p = 0.013$) (Fig. 11A) and between the CIA and M_{cera} ($r^2 = 0.28$, $p = 0.0038$) (Fig. 11B).

Moreover, on single regression analysis, the CIA/ SIA, which was an index of the ceramide content per unit stratum corneum, was significantly positively correlated to the $M_{\text{cera}}/ M_{\text{prot}}$ ($r^2 = 0.33$, $p = 0.0013$) (Fig. 11C).

3.3 Ceramide amount regression using deep learning

Figure 12 shows the comparisons between the results of regression prediction for the protein and ceramide contents using the CNN and the observed values. The correlation coefficients were $r^2 = 0.78$ and $r^2 = 0.66$, respectively ($p < 0.001$ for both). The protein content prediction from the model using the brightfield images showed a narrow range of values. Figure 12C shows the estimation of the ceramide-to-protein content ratio. The simple predictive ceramide-to-protein content ratio correlated with the observed ratio ($r^2 = 0.66$), whereas the ratio predicted from the deep learning regression model using the polarized images correlated with the observed ratio ($r^2 = 0.42$).

In order to understand how the ceramide density was estimated from the polarized images, we applied the Grad-CAM method to the trained model. Fig. 13 demonstrates a comparison of the original and the heat map, which highlighted the areas that contributed to the output of the regression model. Overall, the cell areas were weakly highlighted, whereas the bright areas in the polarized image, which were considered the lamellar structure of the stratum corneum, were especially strongly highlighted.

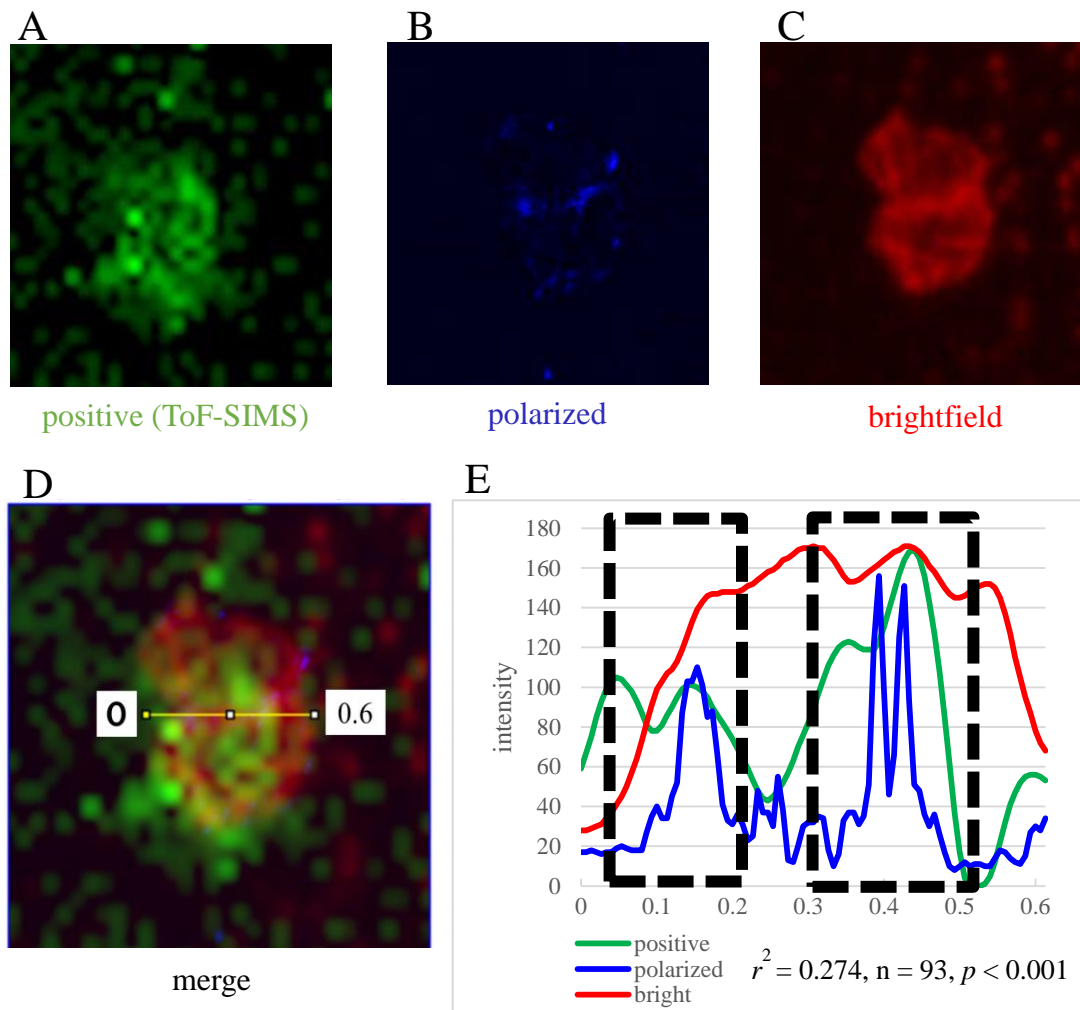


Figure 10. ToF-SIMS imaging analysis. A: ceramide-positive secondary ion peak image (green), B: polarized image (blue), C: brightfield image (red), D: merged image, and E: a graph representing the plot profiles. This represents Pearson coefficients of correlation between positive (red) and polarized images ($r^2 = 0.274$, $n = 93$, $p < 0.001$). ToF-SIMS, time of flight–secondary ion mass spectrometry.

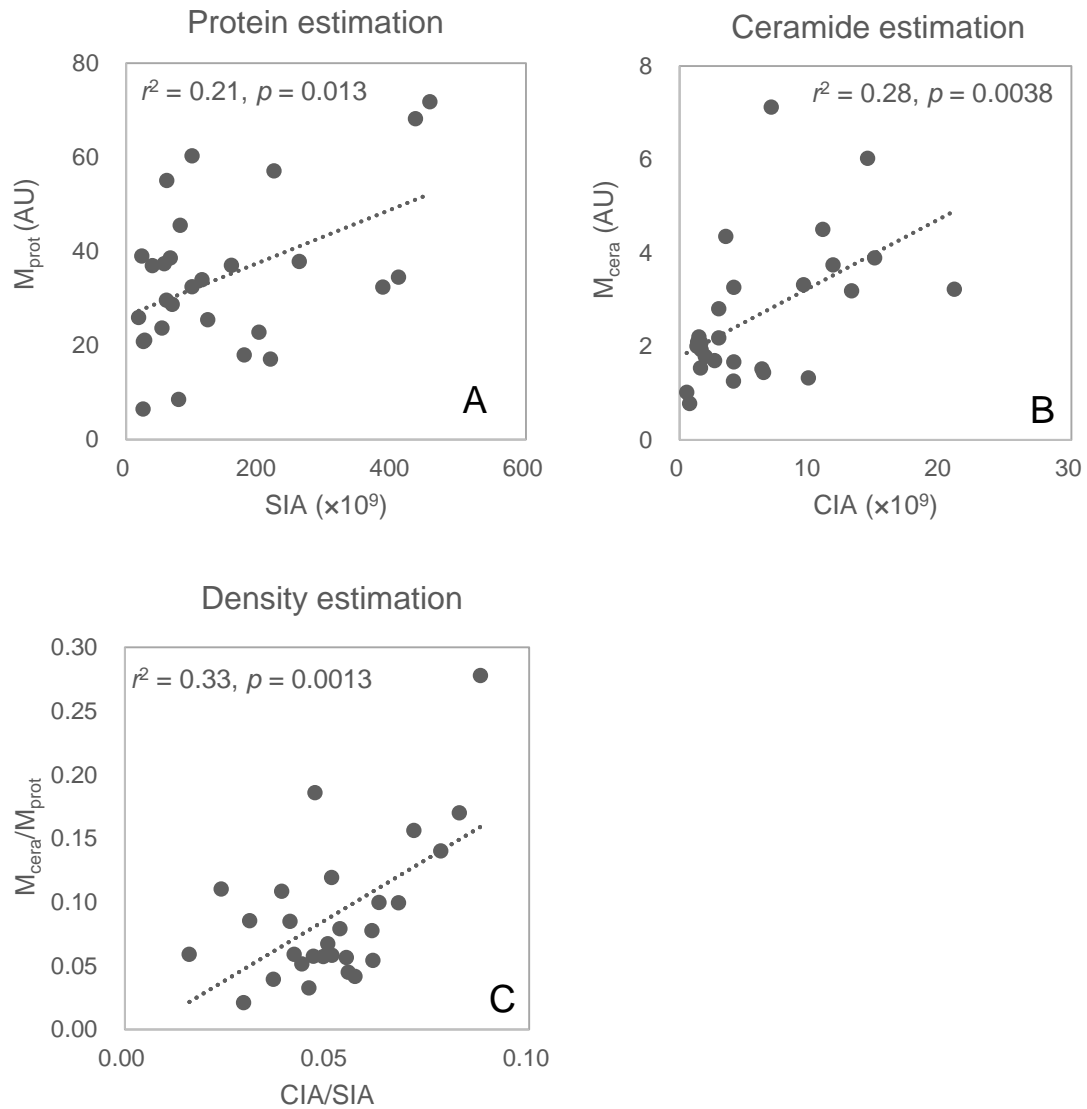


Figure 11. Comparison of the observed and predicted protein and ceramide contents and their ratios. The x axis shows the values predicted from ImageJ, and the y axis shows the observed contents. Black circles represent the average of the values from 125 images. SIA, the Stripping Index of Amount from brightfield images. CIA, the Ceramide Index of Amount from polarized images. M_{prot} , the protein content by BCA Protein Assay. M_{cera} , the ceramide content by HPLC. The r^2 values represent square of Pearson correlation coefficients and the p -values represent their significance.

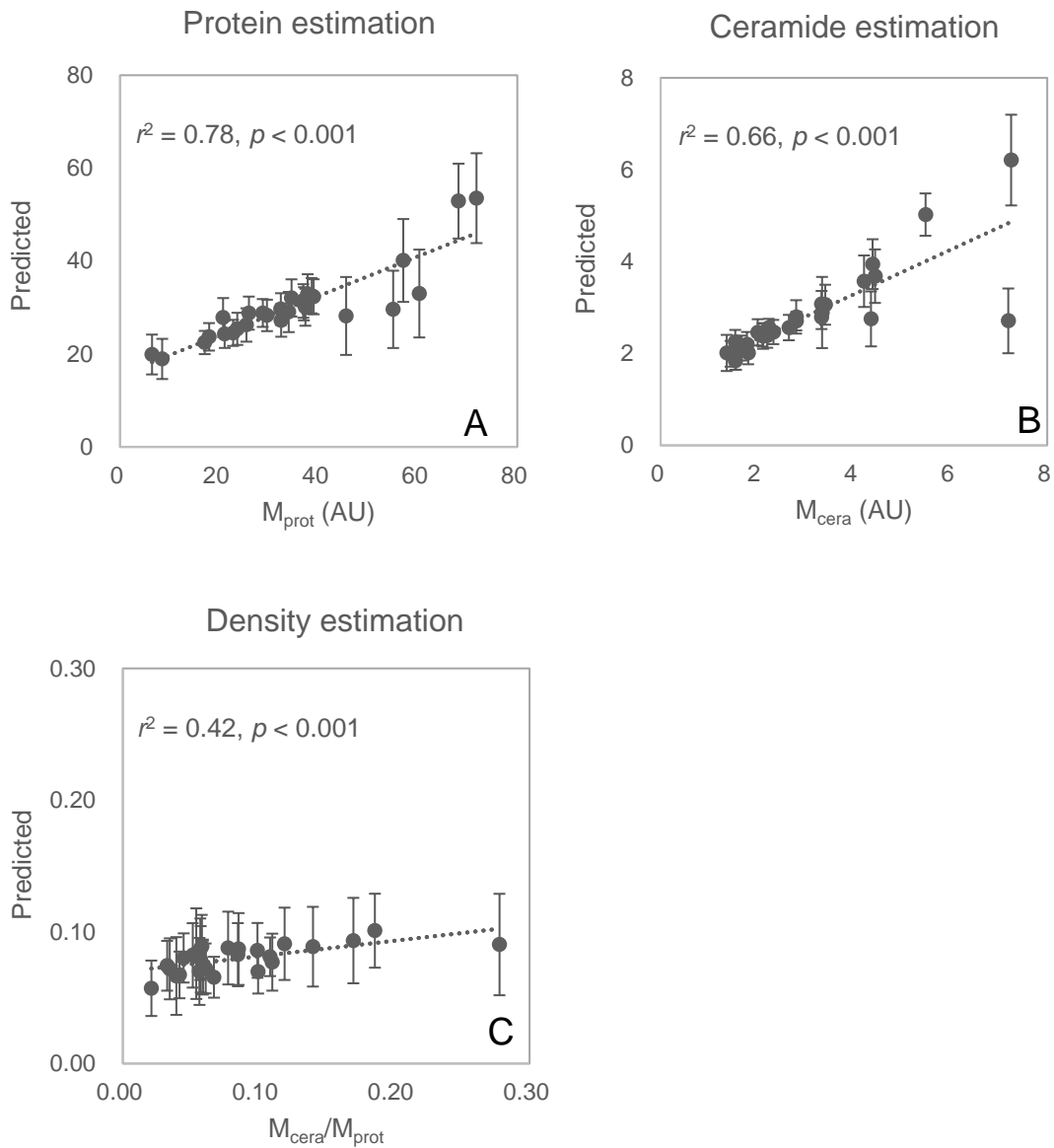


Figure 12. Comparison of the observed and predicted protein and ceramide contents and their ratios. The x axis shows the observed contents, and the y axis shows the values predicted from the regression model. Black circles represent the average, and the error bars represent the standard deviations of the values predicted from 125 images. The r^2 values represent square of Pearson correlation coefficients and the p -values represent their significance.

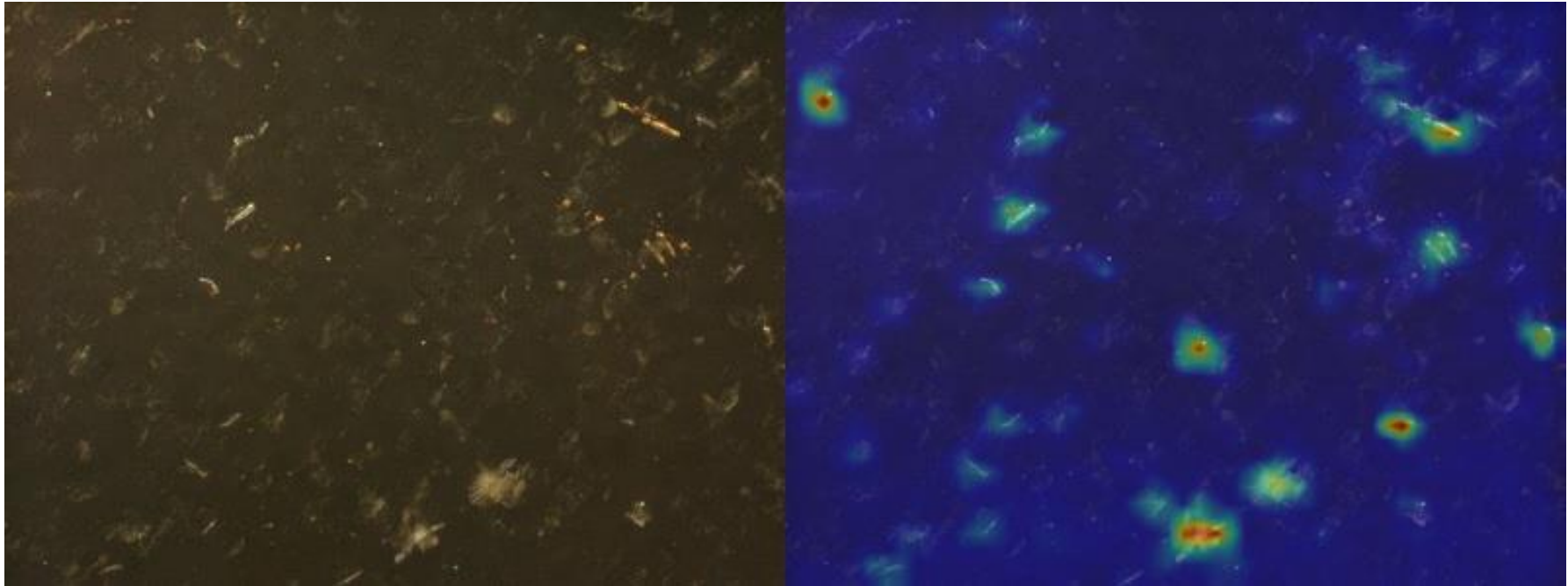


Figure 13. Feature areas highlighted by Grad-CAM. Left: the original polarized image; Right: heat map of the gradation of contribution to the ceramide density estimation. Weak highlights are represented by green, and strong highlights by red.

Chapter 4: Discussion

We expected that the intercellular lipids content could be correlated with the luminance values calculated from polarized images of stratum corneum strips because the lamellar structure of intercellular lipids is polarized.^{48, 49} When a stratum corneum strip collected using the conventional tape stripping method is observed under a polarized microscope, observing only the polarized light emitted by areas with a lamellar structure is not possible. We succeeded in extracting this polarized light mainly by developing a new tool for stratum corneum sampling using a rubber-based adhesive on a glass slide, possibly because rubber-based adhesives and glass do not have an ordered crystal structure,⁵⁷ suggesting the usefulness of materials with similar characteristics.

However, it was unclear whether the polarized light obtained from the stripped stratum corneum was derived solely from the lamellar structure of intercellular lipids, including ceramides, and did not include those that were derived from the overlapping structure of the stratum corneum cells. Excessive multilayer peeling was inhibited because of the weak adhesive strength of the newly developed tape, and the polarization area overlapped with the area where ceramide was detected by ToF-SIMS. Therefore, there seemed to be no problem, considering that the polarized light was mainly derived from the lamellar structure of intercellular lipids, including ceramides.

Meanwhile, the presence of intercellular lipids, which did not sufficiently form a lamellar structure, in the stripped stratum corneum was possible,⁵⁸ and surfactants affect and lead to disorder in the LPP lamellar structure of the human stratum corneum, contributing to barrier damage.^{59, 60} In fact, ceramides were detected by ToF-SIMS in a portion of the unpolarized area. Because of the significant correlation between the polarization intensity and the HPLC-quantified ceramides, our simple method was considered to be useful in the evaluation of intercellular lipids content. Moreover, in our method, a part of disordered intercellular lipids containing ceramide was not considered as clear polarized light, and the lamellar structure might have contributed to the barrier function. Barrier function can be evaluated by TEWL measurement, but the intercellular lipid content, composed of a lamellar structure, should be evaluated by X-ray.^{52, 54} Therefore, although there are several layers to be stripped, our method may easily

evaluate the effect of applying a formulation containing an intercellular lipid component to the skin or washing the skin with a surfactant.

The results of regression analyses implied that the SIA reflected the number of corneocytes, the CIA reflected the ceramide content, and the CIA/SIA reflected the ceramide content per weight of the stratum corneum. The regression models showed that the observed contents were reflected more accurately by the values obtained using deep learning than by those obtained using ImageJ. The narrow range of values for the protein content prediction from the model was possibly because of the high background levels in the brightfield images. Adjustment of the luminance and color inversion of the images may broaden the range. The findings of Grad-CAM method suggested that the density was estimated from both the total cell mass and the ceramide content can be estimated using the polarized images. Notably, when using deep learning, the ceramide content per unit stratum corneum could only be accurately predicted based on the polarized images. Deep learning has been used to support the diagnoses of skin cancer and lung adenocarcinoma^{42, 43} and may be useful in the observation and diagnosis of hair, skin, and scalp problems; in this study, it was proven to be useful for stripped stratum corneum. Model construction may enable quick and practical evaluation of the ceramide content using a polarized image of the stratum corneum. Moreover, ceramides in the stratum corneum greatly contribute to barrier formation by forming the broad lamellar sheets with other intercellular lipids.^{1, 2, 22, 23} In evaluating the epidermal permeability barrier function, the amount intercellular lipids that form the lamellar structure should be measured rather than ceramide content alone. Our proposed method evaluates the lamellar structure of intercellular lipids, thus indicating the usefulness of the values derived from the regression models as indices of the estimated degree of stratum corneum barrier function. From a practical viewpoint, such as skin care, we expect that application of this new tool would enable evaluation of intercellular lipids content in the facial stratum corneum.

The rubber-based materials mixed with resin were used for a long time as an adhesive layer for stripping the stratum corneum (e.g., Cellotape®, Nichiban, Tokyo, Japan)⁶¹ and for the adhesive plaster (e.g., BAND-AID®, Johnson & Johnson, New jersey, USA). Moreover, our tool had an equal or worse adhesive property due to the amount of stripped stratum corneum, compared with that of the commonly used tape for stratum corneum stripping. As an alternative to five times of stripping from the same area, stripping once

or twice from larger areas can provide the required number of microscope images. An equivalent stratum corneum sampling tool is created and available by, for example, dissolving solid natural rubber with toluene, applying it to a glass slide, and drying the solvent.

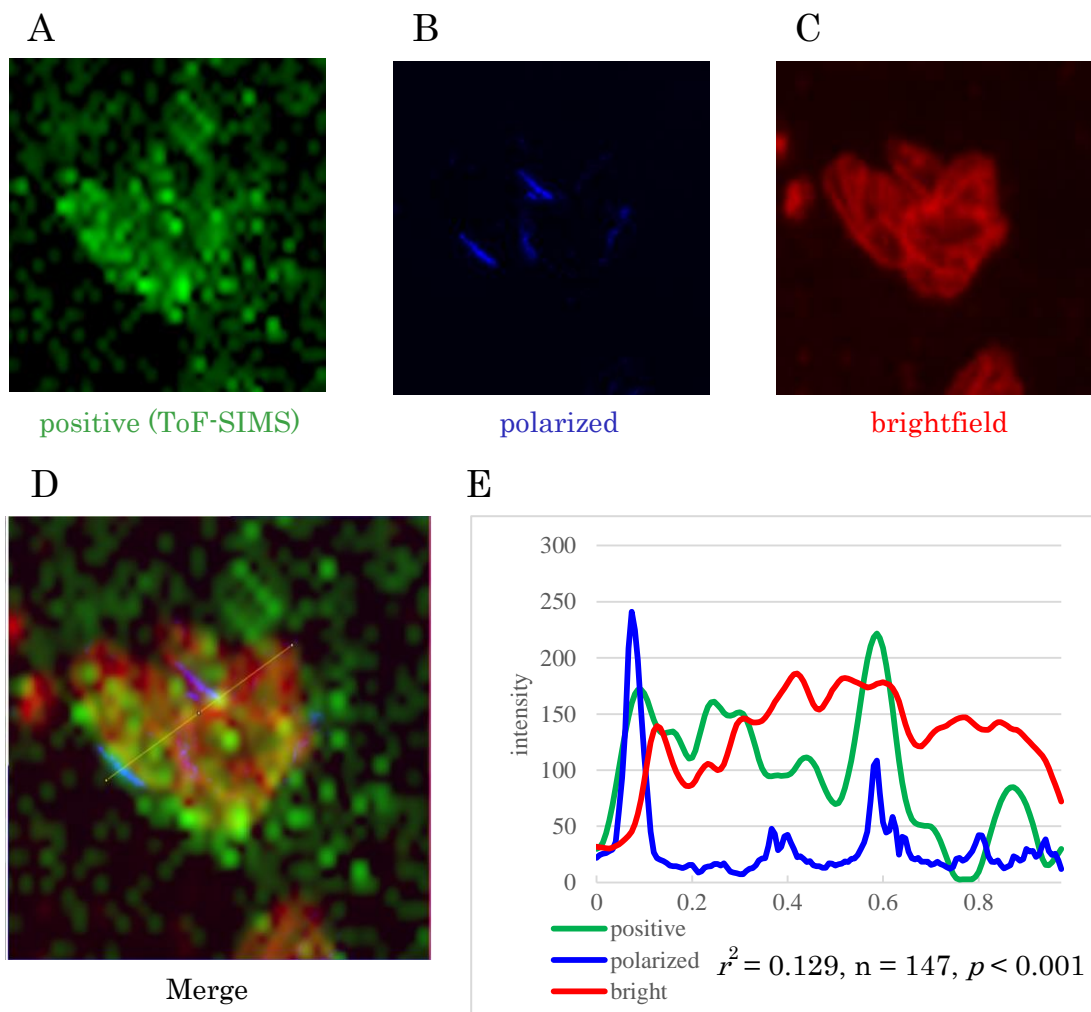
Moreover, although the base material we used was glass slide,³⁷ films (e.g., Triacetylcellulose film) that do not cause unnecessary luminescence and is black on polarized images can be used. Development of a tape that used film as base material would allow ordinary users to more easily apply the tool on the face.

In contrast to conventional methods, this method was simple and nondestructive and did not require an expensive device to be measured by sending the stratum corneum even without visiting and enable efficient evaluation of a large number of specimens. Therefore, this method can be applied not only to evaluate skin conditions and the usefulness of cosmetics in the laboratory but also to check the skin using a tool that is commercially available in stores and on the web. In addition, it may be worth investigating the correlation with the amount of intercellular lipids other than ceramide. Moreover, the method may be helpful for elucidating the role of intercellular lipids with lamellar structures by examining their correlations with other skin condition parameters, such as the water content and TEWL before and after the application of formulation and washing.

In atopic dermatitis, TEWL is high even in eczema-free areas, and it has been related to the ceramide content in the stratum corneum.¹⁹ Our method may be useful for early detection of potential atopic dermatitis patients. The disruption of skin barrier function due to atopic dermatitis may trigger food allergies and other allergic reactions known as the “allergy march.”⁶² The report suggested that peanut allergens absorbed through the skin may cause allergic sensitization. Currently, based on the “Definition and Diagnostic Criteria for AD” prepared by the Japanese Dermatological Association, patients meeting three basic items are regarded as having atopic dermatitis: (i) pruritus; (ii) typical morphology and distribution of the eczema; and (iii) chronic or chronically relapsing course, with chronic or recurrent being defined as more than 2 months for infants and more than 6 months for others.^{63,64} Adequate observation is also necessary to differentiate atopic dermatitis from other diseases such as contact dermatitis. Therefore, this method may be useful as a diagnostic aid for dermatopathological histopathology to verify whether the patient has atopic diathesis at an early stage.

Chapter 5: Conclusion

We developed a simple evaluation method for the intercellular lipid content based on luminance, which was calculated using polarized images of the stratum corneum stripped from the skin surface. Imaging the same area of the sample under a polarizing microscope and ToF-SIMS showed that the presence of ceramide, one of the main components of intercellular lipids, was involved in the polarization brightness. The CIA/SIA index of ceramide content per unit stratum corneum can be useful in the evaluation of the barrier function by an orderly lamellar structure of the stratum corneum. In this study, deep learning provided an accurate predictive ceramide content, which reflected the observed content per unit stratum corneum and was a more suitable index for evaluation. These methods for evaluating intercellular lipids by imaging analysis allow for additional morphological observation and chemical analysis without destroying the sample and for evaluation of large numbers of samples.



Supplementary Figure S1. ToF-SIMS, polarized and brightfield images. A: Ceramide-positive secondary ion peak image (green). B: Polarized image (blue). C: Brightfield (red). D: Merged image. E: Graph representing the plot profiles. This represents Pearson coefficients of correlation between positive (red) and polarized images ($r^2 = 0.129$, $n = 147$, $p < 0.001$). The p-values were calculated by the t-test. ToF-SIMS, time of flight–secondary ion mass spectrometry.

Research Achievement

- The contents of Chapters 2.1, 2.2, 2.3, 3.1, 3.2, and 3.3 were published as: Evaluation of intercellular lipid lamellae in the stratum corneum by polarized microscopy. Naoki Asada, Morita Ryo, Rikae Kamiji, Mami Kuwajima, Masahiko Komorisono, Tatsuo Yamamura, Naoaki Ono, Shigehiko Kanaya, Shuichi Yoshikawa. *Skin research and technology*, 2022;**28**(3):391-401.
- The contents of Chapters 2.1, 2.2, 2.3, 3.2, and 3.3 were presented as: A Novel Non-destructive Ceramides Quantification Method Using Polarizing Microscope Images of Stratum Corneum. Naoki Asada, Rikae Kamiji, Mami Kuwajima, Masahiko Komorisono, Tatsuo Yamamura, Naoaki Ono, Shigehiko Kanaya, Shuichi Yoshikawa. Proceedings of 24th IFSCC Conference 2019 (poster session). The poster was selected for IPCE as a Featured Poster.
- The contents of Chapters 2.1, 2.2, 2.3, 3.2, and 3.3 were presented as: A Novel Non-destructive Ceramides Quantification Method Using Polarizing Microscope Images of Stratum Corneum. Naoki Asada, Rikae Kamiji, Mami Kuwajima, Masahiko Komorisono, Tatsuo Yamamura, Naoaki Ono, Shigehiko Kanaya, Shuichi Yoshikawa. Proceedings of 4th IPCE Conference 2020 (oral session).
- The contents of Chapters 2.1, 2.2, 2.3, 3.1, 3.2, and 3.3 were presented as: Evaluation of intercellular lipid lamellae in the stratum corneum by polarized microscopy. Naoki Asada, Morita Ryo, Rikae Kamiji, Mami Kuwajima, Masahiko Komorisono, Tatsuo Yamamura, Naoaki Ono, Shigehiko Kanaya, Shuichi Yoshikawa. Proceedings of 8th EPHAR Congress 2021 (poster session).

Acknowledgment

I would like to express my deepest gratitude to Professor Kanaya and members of Kanaya Laboratory in Nara Institute of Science and Technology. I think that Professor Kanaya's spirit of academic inquiry and attitude toward research should be emulated as my future way of life as a researcher.

I deep thank to Associate Professor Ono for the politely research in the ceramide amount regression using deep learning. Dr. Ono's technology has greatly contributed to the development of ceramide image evaluation.

I deep thank to Dr. Ming Huang and Dr. Md. Altaf-Ul-Amin for their assistance in writing the paper.

I would like to express my deep gratitude to everyone at Kobayashi Pharmaceutical Co., Ltd. for giving me this research opportunity. I would like to deeply thank to Mr. Shuichi Yoshikawa, Mr. Tatsuo Yamamura, Mr. Masahiko Komorisono, Mrs. Rikae Kamiji, Mrs. Mami Kuwajima, Mr. Ryo Morita, Miss Midori Kushima, Mrs. Kiyoko Tojima and Mr. Yasuyuki Hasegawa.

Finally, I thank my son (Sota), daughter (Miori) and wife (Chisato) for supporting my research activities for many years.

Reference

1. Narangifard A, Wennberg CL, den Hollander L et al. Molecular reorganization during the formation of the human skin barrier studied in situ. *J Invest Dermatol.* 2021;141:1243-1253.e6.
2. Harding CR. The stratum corneum: structure and function in health and disease. *Dermatol Ther.* 2004;17:6-15.
3. Fujii M. The Pathogenic and Therapeutic Implications of Ceramide Abnormalities in Atopic Dermatitis. *Cells.* 2021;10(9):2386.
4. Kurata N, Akiyama H, Hosoya H, Aoki H, Ishikawa K, Marunouchi T. Mutations in the v-mos gene abolish its ability to induce differentiation but not transformation. *Eur J Cell Biol.* 1995;68(1):55-61.
5. Elias PM, McNutt NS, Friend DS. Membrane alterations during cornification of mammalian squamous epithelia: a freeze-fracture, tracer, and thin-section study. *Anat Rec.* 1977;189(4):577-594.
6. Masukawa Y, Narita H, Shimizu E, Kondo N, Sugai Y, Oba T, Homma R, Ishikawa J, Takagi Y, Kitahara T, Takema Y, Kita K. Characterization of overall ceramide species in human stratum corneum. *Journal of lipid research.* 2008;49(7):1466–1476.
7. van Smeden J, Hoppel L, van der Heijden R, Hankemeier T, Vreeken RJ, Bouwstra JA. LC/MS analysis of stratum corneum lipids: ceramide profiling and discovery [published correction appears in *J Lipid Res.* 2017 Feb;58(2):479]. *J Lipid Res.* 2011;52(6):1211-1221
8. Masukawa Y, Tsujimura H. Highly sensitive determination of diverse ceramides in human hair using reversed-phase high-performance liquid chromatography-electrospray ionization mass spectrometry. *Lipids.* 2007;42(3):275-290.
9. Kihara A. Synthesis and degradation pathways, functions, and pathology of ceramides and epidermal acylceramides. *Prog Lipid Res.* 2016;63:50-69.
10. Hill JR, Wertz PW. Molecular models of the intercellular lipid lamellae from epidermal stratum corneum. *Biochim Biophys Acta.* 2003;1616(2):121-126.
11. Abraham W, Downing DT. Preparation of model membranes for skin permeability studies using stratum corneum lipids. *J Invest Dermatol.*

- 1989;93(6):809-813.
12. Nakazawa H, Fukunaga K, Sakai S, Yakumaru M, Sumida Y, Inoue S. Characteristics of β -Galactosyl-L-serine-diamides in reinforcing the SC lamellar structure. *J. Jpn. Cosmet. Sci. Soc.* 2005;29(2):103-108.
 13. Madison KC, Swartzendruber DC, Wertz PW, Downing DT. Presence of intact intercellular lipid lamellae in the upper layers of the stratum corneum. *J Invest Dermatol.* 1987;88(6):714-718.
 14. Swartzendruber DC, Wertz PW, Kitko DJ, Madison KC, Downing DT. Molecular models of the intercellular lipid lamellae in mammalian stratum corneum. *J Invest Dermatol.* 1989;92(2):251-257.
 15. Hou SY, Mitra AK, White SH, Menon GK, Ghadially R, Elias PM. Membrane structures in normal and essential fatty acid-deficient stratum corneum: characterization by ruthenium tetroxide staining and x-ray diffraction. *J Invest Dermatol.* 1991;96(2):215-223.
 16. Hölzle E, Plewig G. Effects of dermatitis, stripping, and steroids on the morphology of corneocytes. A new bioassay. *J Invest Dermatol.* 1977;68(6):350-356.
 17. Watanabe M, Tagami H, Horii I, Takahashi M, Kligman AM. Functional analyses of the superficial stratum corneum in atopic xerosis. *Arch Dermatol.* 1991;127(11):1689-1692.
 18. Kumagai H, Watanabe H, Kozu T, Noguchi H, Takahashi M. Physiological and morphological changes in facial skin with ageing (I). Age-related changes in the skin of Japanese women. *J Soc Cosmet Chem Japan* 1989;23:9-21.
 19. Imokawa G. Ceramides as natural moisturizing factors and their efficacy in dry skin. In: Leyden JJ, Rawlings AV, eds. *Skin Moisturization*. 1st ed. New York: Marcel Dekker; 2002.
 20. Kikuchi K, Tagami H; Japanese Cosmetic Scientist Task Force for Skin Care of Atopic Dermatitis. Noninvasive biophysical assessments of the efficacy of a moisturizing cosmetic cream base for patients with atopic dermatitis during different seasons. *Br J Dermatol.* 2008;158(5):969-978.
 21. Strese H, Kuck M, Benken R, et al. Application of optical methods to characterize textile materials and their influence on the human skin. *J Biomed Opt.* 2011;16(4):046013.

22. Vergou T, Schanzer S, Richter H, et al. Comparison between TEWL and laser scanning microscopy measurements for the in vivo characterization of the human epidermal barrier. *J Biophotonics*. 2012;5(2):152-158.
23. Bouwstra JA, Gooris GS, van der Spek JA, Bras W. Structural investigations of human stratum corneum by small-angle X-ray scattering. *J Invest Dermatol*. 1991;97:1005-1012.
24. Bouwstra JA, Gooris GS, Vries MAS, van der Spek JA, Bras W. Structure of human stratum corneum as a function of temperature and hydration: A wide-angle X-ray diffraction study. *International Journal of Pharmaceutics*. 1992;84:205-216.
25. Nakazawa H, Ohta N, Hatta I. A possible regulation mechanism of water content in human stratum corneum via intercellular lipid matrix. *Chem Phys Lipids*. 2012;165(2):238-243.
26. Ponec M, Gibbs S, Pilgram G, et al. Barrier function in reconstructed epidermis and its resemblance to native human skin. *Skin Pharmacol Appl Skin Physiol*. 2001;14 Suppl 1:63-71.
27. Bouwstra JA, Gooris GS, Dubbelaar FE, Weerheim AM, Ijzerman AP, Ponec M. Role of ceramide 1 in the molecular organization of the stratum corneum lipids. *J Lipid Res*. 1998;39(1):186-196
28. Bouwstra JA, Honeywell-Nguyen PL, Gooris GS, Ponec M. Structure of the skin barrier and its modulation by vesicular formulations. *Prog Lipid Res*. 2003;42(1):1-36.
29. Hatta I. Skin Bioscience : Structure and Function of Stratum Corneum. *Journal of the Adhesion Society of Japan*. 2016;52(5):145-151.
30. Charalambopoulou GC, Steriotis TA, Hauss T, Stubos AK, Kanellopoulos NK. Structure alterations of fully hydrated human stratum corneum. *Physica B* 2004;350(1-3):e603-606.
31. Hatta I, Ohta N, Inoue K, Yagi N. Coexistence of two domains in intercellular lipid matrix of stratum corneum. *Biochim Biophys Acta*. 2006;1758(11):1830-1836.
32. Pilgram GS, Vissers DC, van der Meulen H, et al. Aberrant lipid organization in stratum corneum of patients with atopic dermatitis and lamellar ichthyosis. *J Invest Dermatol*. 2001;117(3):710-717.
33. Janssens M, Mulder AA, Van Smeden J et al. Electron diffraction study of

- lipids in non-lesional stratum corneum of atopic eczema patients. *Biochim Biophys Acta*. 2013;1828:1814-1821.
34. Caspers PJ, Lucassen GW, Wolthuis R, Bruining HA, Puppels GJ. In vitro and in vivo Raman spectroscopy of human skin. *Biospectroscopy*. 1998;4:S31-S39.
 35. Caspers PJ, Lucassen GW, Carter EA, Bruining HA, Puppels GJ. In vivo confocal Raman microspectroscopy of the skin: noninvasive determination of molecular concentration profiles. *J Invest Dermatol*. 2001;116:434-442.
 36. Imokawa G, Kuno H, Kawai M. Stratum corneum lipids serve as a bound-water modulator. *J Invest Dermatol*. 1991;96:845-851.
 37. Imokawa G, Abe A, Jin K, Higaki Y, Kawashima M, Hidano A. Decreased level of ceramides in stratum corneum of atopic dermatitis: an etiologic factor in atopic dry skin? *J Invest Dermatol*. 1991;96:523-526.
 38. Jungersted JM, Scheer H, Mempel M et al. Stratum corneum lipids, skin barrier function and filaggrin mutations in patients with atopic eczema. *Allergy*. 2010;65:911-918.
 39. Yano M, Kishida E, Muneyuki Y, Masuzawa Y. Quantitative analysis of ceramide molecular species by high performance liquid chromatography. *J Lipid Res*. 1998;39:2091-2098.
 40. Munir K, Elahi H, Ayub A, Frezza F, Rizzi A. Cancer Diagnosis Using Deep Learning: A Bibliographic Review. *Cancers (Basel)*. 2019;11(9):1235-1270.
 41. Das K, Cockerell CJ, Patil A, et al. Machine Learning and Its Application in Skin Cancer. *Int J Environ Res Public Health*. 2021;18(24):13409-13418.
 42. Brinker TJ, Hekler A, Utikal JS et al. Skin cancer classification using convolutional neural networks: systematic review. *J Med Internet Res*. 2018;20:e11936.
 43. Eguchi R, Ono N, Hirai Morita A et al. Classification of alkaloids according to the starting substances of their biosynthetic pathways using graph convolutional neural networks. *BMC Bioinformatics*. 2019;20:380.
 44. Salah S, Colomb L, Benize AM, et al. Prediction of treatment effect perception in cosmetics using machine learning. *J Biopharm Stat*. 2021;31(1):55-62.
 45. Jiang R, Kezele I, Levinshtein A, et al. A new procedure, free from human

- assessment that automatically grades some facial skin structural signs. Comparison with assessments by experts, using referential atlases of skin ageing. *Int J Cosmet Sci.* 2019;41(1):67-78.
46. Elias PM. Lipids and the epidermal permeability barrier. *Arch Dermatol Res.* 1981;270:95-117.
 47. Elias PM. Epidermal lipids, barrier function, and desquamation. *J Invest Dermatol.* 1983;80:44s-49s.
 48. Akasaki S, Minematsu Y, Yoshizuka N, Imokawa G. The role of intercellular lipids in the water-holding properties of the stratum corneum—recovery effect on experimentally induced dry skin. *Nihon Hifuka Gakkai Zasshi.* 1988;98:41-51.
 49. Silva CL, Nunes SCC, Eusébio MES, Sousa JJS, Pais AACC. Study of human stratum corneum and extracted lipids by thermomicroscopy and DSC. *Chem Phys Lipids.* 2006;140:36-47.
 50. Sjövall P, Skedung L, Gregoire S, Biganska O, Clément F, Luengo GS. Imaging the distribution of skin lipids and topically applied compounds in human skin using mass spectrometry. *Sci Rep.* 2018;8:16683.
 51. Zama K, Okino N, Ito M. Simultaneous quantification of glucosylceramide and galactosylceramide by HPLC. *GlycoPOD.* <https://jcgddb.jp/GlycoPOD/protocolShow.action?nodeId=t139>. Accessed 2019/6/20; 2016.
 52. Matsumoto M, Hayashi S, Arai S. Evaluation of the stratum corneum exfoliated by tape stripping method (No. 1). *J Soc Cosmet Chem Japan.* 1997;32:33-42.
 53. Krizhevsky A, Sutskever I, Hinton GE. ImageNet classification with deep convolutional neural networks. *Commun ACM.* 2017;60:84-90.
 54. Russakovsky O, Deng J, Su H et al. Imagenet large scale visual recognition challenge. *Int J Comput Vis.* 2015;115:211-252.
 55. Kingma DP, Ba JA. A method for stochastic optimization. *arXiv Preprint, arXiv:1412.6980* 2014.
 56. Selvaraju RR, Cogswell M, Das A, Vedantam R, Parikh D, Batra D. Grad-cam: visual explanations from deep networks via gradient-based localization. *Proc IEEE Int Conf Comput Vis.* 2017;618-626.

57. Cangialosi D. Dynamics and thermodynamics of polymer glasses. *J Phys Condens Matter*. 2014;26:153101.
58. Hatta I, Ohta N, Nakazawa H. A possible percutaneous penetration pathway that should be considered. *Pharmaceutics*. 2017;9:26.
59. Bouwstra JA, Dubbelaar FE, Gooris GS, Ponc M. The lipid organisation in the skin barrier. *Acta Derm Venereol Suppl (Stockh)*. 2000;208:23-30.
60. Yanase K, Hatta I. Disruption of human stratum corneum lipid structure by sodium dodecyl sulphate. *Int J Cosmet Sci*. 2018;40:44-49.
61. Kashibuchi N, Muramatsu Y. Exfoliative cytology for morphological evaluation of skin. *J Soc Cosmet Chem*. 1989;1:55-57.
62. Yamamoto-Hanada K, Kobayashi T, Williams HC, et al. Early aggressive intervention for infantile atopic dermatitis to prevent development of food allergy: a multicenter, investigator-blinded, randomized, parallel group controlled trial (PACI Study)-protocol for a randomized controlled trial. *Clin Transl Allergy*. 2018;8:47. Published 2018 Nov 23.
63. Katayama I, Aihara M, Ohya Y, et al. Japanese guidelines for atopic dermatitis 2017. *Allergol Int*. 2017;66(2):230-247.
64. Katoh N, Ohya Y, Ikeda M, et al. Japanese guidelines for atopic dermatitis 2020. *Allergol Int*. 2020;69(3):356-369.